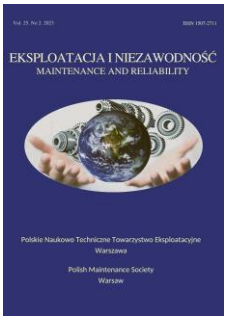

Eksploatacja i Niezawodnosc – Maintenance and Reliability
Volume 28 (2026), Issue 3
journal homepage: http://www.ein.org.pl

Article citation info:
Dong R, Yao Y, Kang Y, Jia X, Ji F, Cao A, Hybrid metaheuristic optimisation algorithms with least-squares support vector machine and stagnation counter for prediction vibration induced by tunnel blasting, Eksploatacja i Niezawodnosc – Maintenance and Reliability 2026: 28(3) http://doi.org/10.17531/ein/218132

Hybrid metaheuristic optimisation algorithms with least-squares support vector machine and stagnation counter for prediction vibration induced by tunnel blasting

Indexed by: Web of Science Group

Runlong Dong[a], Yingkang Yao[a,*], Yize Kang[b], Xiaoyu Jia[a], Fuquan Ji[c], Ang Cao[c]

[a] State Key Laboratory of Precision Blasting, Jianghan University, Wuhan 430056, China
[b] School of Civil Engineering, Sun Yat-Sen University, Zhuhai, 519082, China
[c] CCCC Second Harbor Engineering Company Ltd., Wuhan, 430040, China

Highlights

- A novel ASWOA optimizes is developed for model parameter optimisation.
- Introduces stagnation counters and decay coefficients to boost diversity and global search.
- Proposes a dynamic adaptive stagnation strategy enhancing performance stability.

Abstract

Ground vibrations induced by tunnel blasting can severely impact nearby infrastructure. Therefore, accurate prediction of peak particle velocity (PPV) is essential for ensuring structural safety and engineering sustainability. This study proposes a PPV prediction model based on the Least Squares Support Vector Machine (LSSVM), optimised by a novel Adaptive Stagnation Whale Optimisation Algorithm (ASWOA). To address the limitations of the conventional WOA, a regionally dynamic threshold adjustment strategy based on stagnation counter is proposed. recording the number of consecutive iterations without improvement, and calculate the dynamic threshold by combining the decay coefficient to control the rate of change, thereby adaptively adjusts the trigger probability of spiral updates, improving global search capability. Compared with others models, the proposed method not only improves prediction accuracy but also ensure higher reliability in vibration prediction. Moreover, it provides an efficient tool for vibration control in tunnel blasting under complex geological conditions.

Keywords
tunnel blasting, vibration prediction, stall counter, whale optimisation algorithm, least squares support vector machine

1. Introduction

Drilling and blasting is a widely used method for rock excavation in railway tunnel engineering. However, this process inevitably induces environmental disturbances. Among these, blasting-induced vibration is the most significant [1–4]. The peak particle velocity (PPV) is widely adopted as the key metric to quantify vibration intensity and assess potential damage. So, accurate PPV prediction is essential for blast design optimization and vibration mitigation.

Reliability assessment is a fundamental requirement for vibration prediction, as inaccurate prediction may jeopardise the safety of surrounding infrastructure. However, reliable PPV prediction is difficult owing to the strongly non-linear, strongly coupled interactions among geology, blasting design and site topography. Traditional empirical models, such as the Sadowski

(*) Corresponding author.
E-mail addresses: R. Dong (ORCID: 0009-0005-0118-7844) 13782325360@163.com, Y. Yao (ORCID: 0000-0002-4613-4552) shanxiyao@jhun.edu.cn, Y. Kang (ORCID: 0009-0001-8834-1154) k13283434922@163.com, X. Jia, jiaxy77@163.com, F. Ji, 573036415@qq.com, A. Cao, 1135372402@qq.com

formula and the U.S. Bureau of Mines scaled-distance relationship [5–8], typically consider only linear relationships between PPV and a few major factors (e.g., charge mass and distance). These models fail to account for complex rock mass heterogeneity and the dynamics of blast energy propagation, often resulting in significant prediction errors and inadequate reliability in practical engineering applications, especially in complex tunnel environments.

In recent years, support vector machines, artificial neural networks, and ensemble regression techniques have been increasingly adopted to predict peak particle velocity (PPV) in blasting operations [9–16]. Zhang Guopeng et al. [17] enhanced the performance of the Least Squares Support Vector Machine (LSSVM) through parameter tuning, enabling it to perform more effectively under complex geological conditions. Weisu Weng et al. [18] proposed a dynamic ensemble model that adjusts model weights using a reciprocal error weighting method, leading to better prediction accuracy. Xu et al. [19] applied principal component analysis (PCA) to reduce data redundancy and dimensionality. They built a PCA-SVM model based on this preprocessing step. However, these methods typically rely on grid search, cross-validation, or empirical tuning to determine hyperparameters, making it difficult to find optimal configurations within high-dimensional parameter spaces. This results in constrained model generalisation capabilities.

To address these limitations, researchers have increasingly combined meta-heuristic algorithms with machine learning to optimise hyperparameters [20–24]. Liu et al. [25] developed an evolutionary information-based multi-objective particle swarm optimisation(EIGMOPSO) method to tackle trajectory optimisation and reliability challenge in robotic systems. Bui et al. [26] integrated the moth–flame optimisation (MFO) algorithm with fuzzy neural networks to predict vibration velocity induced by open-pit mine blasting. Hosseini et al. [27] developed a long short-term memory (LSTM) model optimised using the Black Hole algorithm, demonstrating robust performance in ground vibration prediction. Zhou et al. [28] constructed FS-RF and FS-BN models through feature selection techniques to enhance the accuracy of quarry blasting vibration prediction. Huang et al. [29] compared the performance of the TSO, WOA, and CS in hyperparameter optimisation for support vector regression, finding that while WOA excelled in complex scenarios, it was prone to premature convergence—a common flaw in many optimisation algorithms. Specifically, the WOA algorithm frequently traps populations in suboptimal local regions during the early stages of optimisation, resulting in the loss of global search capability. This stems from the algorithm's lack of a mechanism to dynamically adjust search strategies based on the population's evolutionary state. Although prior research has attempted improvements through chaotic mappings or adaptive weights, these approaches primarily tweak control parameters without fundamentally altering how the algorithm explores the solution space. Consequently, their robustness remains inadequate when processing high-dimensional, high-noise practical blasting vibration data.

In summary, current tunnel blasting vibration prediction models exhibit several limitations: empirical models assume linear relationships between PPV and factors such as charge weight and distance from blasting center to monitored point, while neglecting rock mass heterogeneity and blasting energy dynamics. This leads to substantial errors and low reliability in complex tunneling environments; traditional machine learning models rely on grid search or empirical tuning, struggling to identify optimal hyperparameters in high-dimensional spaces and thus limiting generalisation; Meta-heuristic hybrid models can automatically optimise hyperparameters, yet their performance is constrained by common shortcomings inherent to meta-heuristic optimisation algorithms. When applied to high-dimensional, noisy, multi-modal blasting vibration data, most algorithms (including WOA, PSO, CS, etc.) are highly susceptible to local optima, leading to premature convergence and rapid loss of population diversity. Although prior research has attempted improvements through methods such as chaotic mapping or adaptive weighting, these strategies merely adjust control parameters without addressing this core design flaw. Consequently, there is an urgent need for a novel mechanism capable of adaptively adjusting search behaviour based on the evolutionary state of the population, thereby simultaneously enhancing global exploration and local exploitation capabilities.

To address these issues, this study proposes a behavior-driven stagnation detection mechanism that dynamically switches between spiral encircling and prey avoidance behaviors based on fitness trends. Integrating this mechanism

forms the adaptive spiral whale optimization lgorithm (ASWOA), coupled with PCA-reduced LSSVM to establish the ASWOA–LSSVM hybrid model for tunnel blasting vibration prediction. The contributions of this paper are as follows:

(1) A novel stagnation detection mechanism based on behavioural reconstruction strategy is proposed. This mechanism abandons reliance on traditional parameter adjustments, dynamically determining stagnation states by monitoring trends in fitness changes. It adaptively switches between spiral circling and predator avoidance behaviours to achieve a balance between exploration and exploitation.

(2) A hybrid ASWOA-LSSVM prediction model is proposed, which employs PCA for feature dimensionality reduction and utilises ASWOA to optimise LSSVM hyperparameters, thereby significantly enhancing prediction stability under geological uncertainty.

(3) Validated on mountain tunnel blasting data from China's Central Yunnan Water Diversion and Shennan High-Speed Railway projects, the model significantly reduces prediction errors in complex geology, enabling precise vibration control for engineering applications.

2. Principles of the Improved Whale Optimisation Algorithm

2.1. The Whale Optimisation Algorithm

The Whale Optimisation Algorithm (WOA) is an intelligent optimisation algorithm characterised by a simple structure and a small number of parameters. It is designed to simulate the bubble-net hunting strategy of humpback whales. The algorithm mainly consists of two stages: the exploration phase and the exploitation (or feeding) phase.

The algorithm treats the best candidate solution identified during the iteration process as the current optimal solution and guides the search agents to move randomly towards the global optimum based on its position. Once the current optimal solution is determined, the positions of the remaining search agents are dynamically updated using a specific strategy based on changes in their position vectors. In the exploitation phase, two mechanisms are employed: the shrinking encircling mechanism and the spiral position updating mechanism, both of which are mathematically formulated as follows:

$$X(t+1)=\begin{cases} X^*(t)-A\cdot D & ,|A|<1, p<0.5 \\ D'\cdot e^{bl}\cdot cos(2\pi l)+X^*(t) & ,p\geq 0.5 \end{cases} \quad (1)$$

where p is a random number in the range [0, 1]; X denotes the position vector of a search agent; X^* represents the position vector of the current best solution, which is updated at each iteration; $D=|C\cdot X^*(t)-X(t)|$, where A and C are coefficient vectors defined as $A=2a\cdot r-a$ and $C=2\cdot r$, with a being the convergence factor that decreases linearly over iterations, and r being a random number in [0, 1]; $D' = |X*(t) - X(t)|$ represents the absolute distance between a search agent and the best solution.

2.2. Principles of Whale Optimisation Algorithm for Adaptive Stall Detection

Based on the fundamental principle of the Whale Optimisation Algorithm, the original version used a fixed probability (p=0.5) to randomly select the shrinking encircling and spiral update mechanisms during the exploitation phase. However, this static selection strategy shows limited adaptability when applied to complex optimisation tasks, such as the prediction of blast-induced vibrations. Once thealgorithm falls into a local optimum, it is unable to dynamically adjust the exploration probability, thus limiting its global search capability and reducing its efficiency in solving high-dimensional, non-linear problems.

Therefore, this study introduces a stagnation counter mechanism to enhance the algorithm's global exploration capability. Specifically, when the algorithm fails to achieve improvement over several consecutive iterations, the threshold parameter θ that governs the selection of the shrinking encircling mechanism is adaptively reduced. This adjustment increases the likelihood of triggering the spiral updating mechanism. The improvement procedure of the proposed algorithm is outlined as follows:

(1) Stall counter design:

First, define $f_{max}(t)$ as the optimal fitness value at the t-th iteration. A stagnation countera $C(t)$ is introduced, and its update rule is defined as follows:

$$C(t)=\begin{cases} C(t-1)+1, & f_{max}(t)\leq f_{max}(t-1) \\ 0 & , f_{max}(t)>f_{max}(t-1) \end{cases} \quad (2)$$

Where $f_{max}(t)$ represents the best fitness value at the t-th iteration, the stagnation counter $C(t)$ records the number of

consecutive iterations without improvement since the last fitness update of the fitness value. Initially, $C(0)$ is set to 0. At each iteration, the current best fitness value $f_{max}(t)$ is compared with that from the previous iteration $f_{max}(t-1)$, If no improvement is detected, $C(t)$ is incremented by one; otherwise, it is reset to 0 when a better solution is identified. The role of $C(t)$ is to dynamically balance the trade-off between exploration and exploitation within the algorithm. As $C(t)$ increases, the algorithm gradually shifts towards spiral movement, thereby enhancing global search capabilitier and facilitating escape from local optima.

(2) Adaptive threshold adjustment:

A positive decay parameter $\delta(\delta>0)$ is introduced to control the adjustment rate. The dynamic threshold is then calculated as follows:

$$\theta(t) = max(0.5 - \delta \cdot C(t), 0.1) \quad (3)$$

When $C(t)=0$, the threshold $\theta(t)$ is set to 0.5, consistent with the original algorithm. When $C(t)>0$, $\theta(t)$ decreases linearly at a decay rate of δ, but is bounded below by 0.1 to ensure that the algorithm maintains a minimal level of local search capability during prolonged stagnation. The parameter δ controls the decay rate of θ(t), and theoretically can be derived as $\delta=(0.5-\theta_{min})/C_{max}=0.08$. Based on the improved stagnation counter, if $p < \theta(t)$, a contraction encircling strategy is employed; otherwise, a spiral updating mechanism is adopted:

$$X(t+1) = \begin{cases} X^*(t) - A \cdot D & , p < \theta(t) \\ D' \cdot e^{bl} \cdot cos(2\pi l) + \vec{X}^*(t) & , p \geq \theta(t) \end{cases} \quad (4)$$

The enhanced WOA algorithm dynamically adjusting the probability of spiral movement and enhances the adaptability of the predation phase, thereby demonstrating superior performance, particularly in addressing complex optimisation problems.

2.3. Analysis of critical parameters

To investigate how the dynamic threshold varies with the stagnation counter and adjustment rate in the improved Whale Optimisation Algorithm (ASWOA), a parameter sensitivity analysis is conducted using MATLAB. The maximum number of iterations is set to 40. A set of adjustment rates, δ=[0.02, 0.04, 0.06, 0.08, 0.1, 1.0], is defined to represent different sensitivity levels of the dynamic threshold in response to the stagnation counter, as illustrated in Fig. 1. The dynamic threshold is computed using the formula $\theta(t) = \max(0.5 - \delta \cdot C(t), 0)$. To simulate a sequence comprising an initial period of consecutive unsuccessful iterations, followed by improvement and subsequent stagnation, a base pattern of stagnation counter values is defined as base_C_pattern = [0:5, 0, 0:3].

As shown in Fig. 1, the value of $C(t)$ follows a periodic rise and reset pattern, independent of the adjustment rate δ. In the first six iterations, no improvement in the optimal solution is found. Therefore, $C(t)$ gradually increases from 0 to 5. In the seventh iteration, a better solution is identified, At this point, $C(t)$ is reset to 0. A similar cycle then occurs. Over the next four iterations, due to stagnation, $C(t)$ rises from 0 to 3 and then resets again. This repetitive behaviour reflects the alternating phases of stagnation and optimisation in the enhanced WOA algorithm. This suggests that the algorithm can dynamically respond to search stagnation and resume global exploration.

As $C(t)$ increases, the dynamic threshold $\theta(t)$ decreases. The rate of this decrease is controlled by the decay parameter δ. As shown in Fig. 2, a larger δ causes $\theta(t)$ to decrease faster. For example, when $C(t) = 5$ and $\delta = 0.02$, θ(t) gradually decreases from 0.5 to 0.4 in six iterations. When $\delta = 0.04$, $\theta(t)$ falls to 0.3 in the same number of iterations. In contrast, when $\delta = 1.0$, $\theta(t)$ reaches 0 as early as in the first iteration when $C(t) = 1$. These results show that a higher δ leads to faster decrease of $\theta(t)$, thus increasing the likelihood of selecting the spiral search mechanism. This behaviour allows the algorithm to respond faster to stagnation, thus enhancing its global exploration capability.

Fig. 2 illustrates that all curves have the same y-intercept at 0.5. This value representss the initial maximum value of the dynamic threshold at $C(t)=0$. Each curve crosses the x-axis at the theoretical stagnation limit, where $\theta(t)=0$. At this point, the corresponding stagnation counter value is $C_{critical}=0.5/\delta$. As δ increases, the slpoes of the curves become steeper in the negative direction. This indicates that the dynamic threshold becomes more sensitive to changes in $C(t)$.

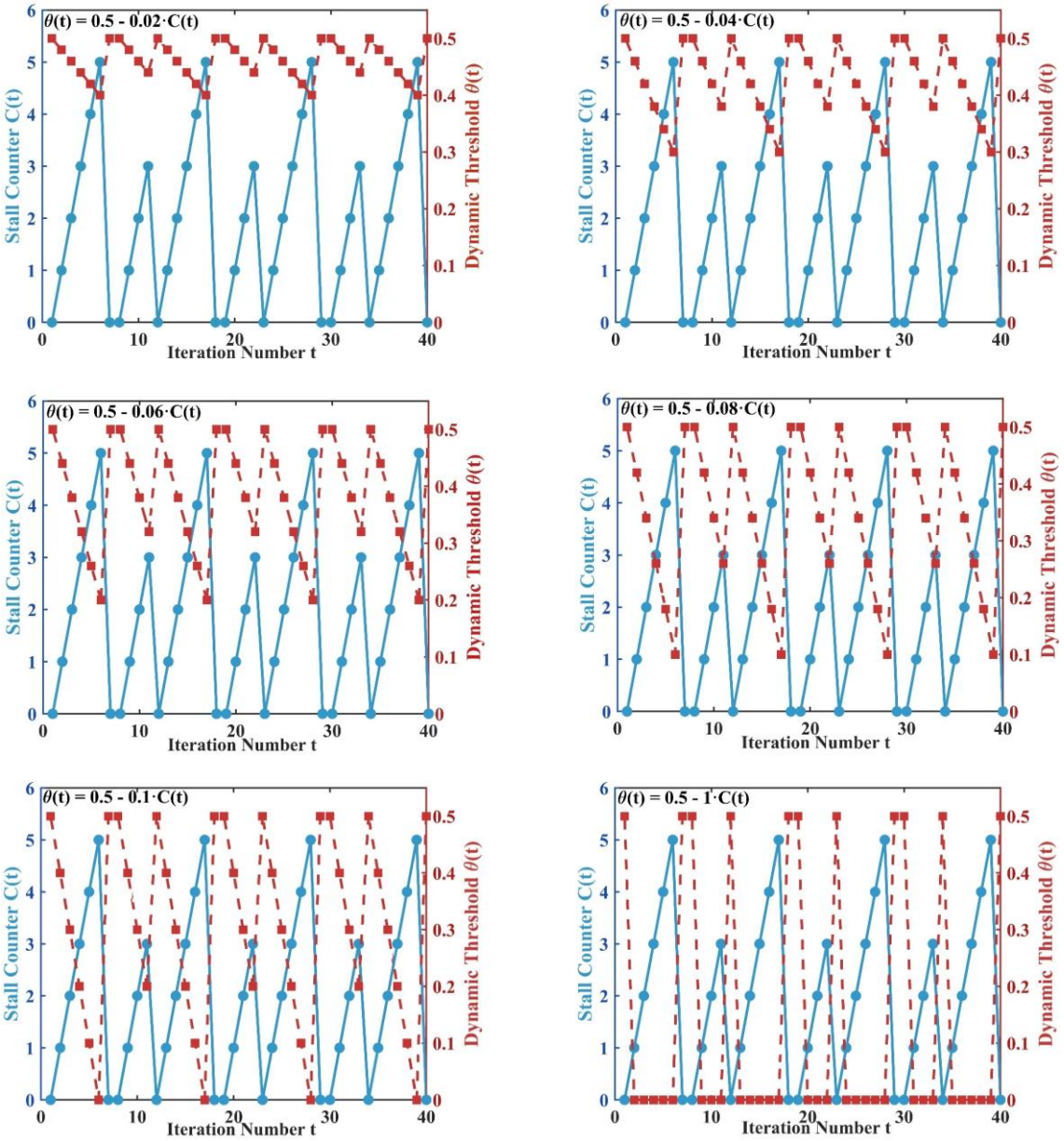

Figure 1. Sensitivity changes during dynamic threshold response stagnation counting at different adjustment rates.

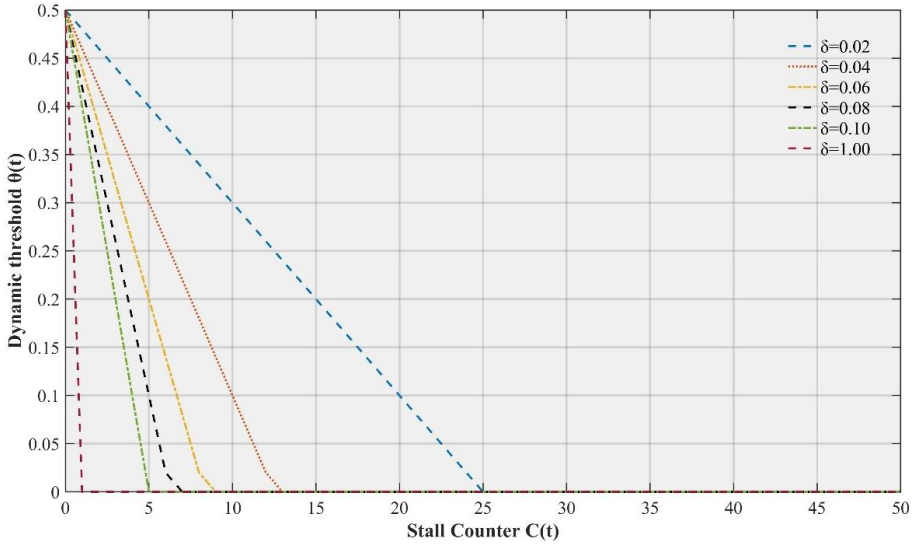

Figure 2. Theoretical change curves of dynamic thresholds under different adjustment rates.

According to the equation $\theta(t)=0.5-\delta \cdot C(t)$, the dynamic threshold is linearly and negatively correlated with the stall counter, with a slope of $-\delta$. In order to quantify the effect of δ, this study calculated the value of the critical $C(t)$, i.e., $Ccritical=0.5/\delta$. At $\theta(t)=0$. The corresponding $C(t)$ is shown in Table 1.

Table 1. Effect of different adjustment rates δ on dynamic threshold critical values.

δ value	Theoretical critical values C(t)	Simulation threshold C(t)
0.02	25.0	5
0.04	12.5	5
0.06	8.3	5
0.08	6.25	5
0.1	5	5
1	0.5	0.5

Specifically, the dynamic threshold $\theta(t)$ decreases linearly with the increase of the stagnation counter $C(t)$, and the rate of this decline is controlled by the adjustment factor δ. The algorithm is able to achieve this by using a number of different thresholds. When $\delta=0.02$, the threshold decreases slowly; for instance, at $C(t)=5$, θ(t) stays at 0.4, indicating that the algorithm still maintains a relatively high probability of employing a contract-wrapping mechanism, thus facilitating local search. On the contrary, when $\delta=1$, $\theta(t)$ drops to 0 immediately after $C(t)\geq 0.5$, causing the algorithm to switch to global search completely. In the simulations, $C(t)\leq 5$ is defined; therefore, when the theoretical value of $C_{\text{critical}}=0.5/\delta$ exceeds 5, the dynamic threshold is not 0, preserving a degree of local search capability.

In summary, a higher value of δ results in a faster decay of $\theta(t)$, thereby increasing the algorithm's tendency towards exploration. Conversely, a smaller δ leads to a higher $\theta(t)$, which promotes exploitation of the current solution and encourages intensification around the best-known optimum.

2.4. Algorithm Performance Testing

Given space constraints, this paper selects eight representative functions from 23 classical benchmark functions to validate the fundamental performance and stability of the proposed ASWOA algorithm. The selected functions span diverse categories to comprehensively examine the algorithm's global exploration capability, local exploitation capability, and convergence stability across multiple search environments. These included the high-dimensional single-peak test functions F1 and F7, the high-dimensional multi-peak test functions F8 and F12, and the fixed-dimensional test functions F15, F19, F21 and F23. Single-peak functions were employed to evaluate the algorithm's convergence speed and solution accuracy, while multi-peak functions were used to examine its global exploration capability. Fixed-dimensional multi-peak functions served to detect the algorithm's balance between global exploration and local optimisation.The specific details of the eight benchmark functions selected are shown in the Table 2.

Table 1. Benchmarking function.

Function numbering	Function name	Value range	Theoretical optimum value
F1	Sphere	$[-100,100]^D$	0
F7	Quartic with noise	$[-1.28,1.28]^D$	0
F8	Schwefel 2.26	$[-5.12,5.12]^D$	$-418.9829 \times D$
F12	Penalized 1	$[-65.53,65.53]^D$	0
F15	Kowalik	$[-5,5]^4$	3.075×10^{-4}
F19	Hartmann-3	$[0,1]^3$	−3.86278
F21	Shekel-5	$[0,10]^4$	−10.1532
F23	Shekel-10	$[0, 10]^4$	−10.5364

This simulation experiment was conducted on a Windows 10 (64-bit) operating system, utilising a hardware environment comprising an Intel Core™ i5-9300H CPU (base frequency 2.40 GHz) and 8 GB of memory. The algorithmic programme was implemented on the MATLAB R2023b platform. To ensure the fairness and validity, all algorithms employed identical parameter settings: population size and maximum iteration count were set to 30 and 400 respectively, with the experimental dimension set to D=10. Furthermore, to mitigate the inherent randomness of heuristic algorithms, each algorithm was independently run 30 times on each test function. The proposed ASWOA algorithm was comparatively analysed against several representative algorithms (WOA, BWO, APO,) across eight benchmark function sets. Due to space constraints, this study selected twelve representative test functions (F1, F7, F8, F12, F15, F19, F21, F23) for detailed analysis. This multi-faceted assessment of algorithmic performance provides a scientific basis for optimising and refining the algorithms. The results are presented in Table 3.

Experimental results demonstrate that the ASWOA algorithm significantly outperforms the other three classical algorithms in key metrics such as finding optimal solutions and stability. Overall, after 30 independent runs, the ASWOA

algorithm achieved the minimum values for optimality, mean, and standard deviation, fully showcasing its outstanding performance in global search and stability. The findings further underscore the markedly enhanced optimization capabilities of the ASWOA algorithm, while validating the efficacy and reliability of adaptive adjustment strategies, such as the introduction of a stagnation counter. This provides fresh insights for subsequent algorithmic refinements and performance enhancements.

Table 3. Benchmark function results.

Function	Indicator	WOA	BFO	APO	ASWOA
F1	Best	6.51E-88	1.29E-08	4.13E-07	5.19E-85
	Std	5.62E-67	1.95E-07	1.63E-06	4.81E-70
	Mean	1.03E-67	1.85E-07	2.12E-06	8.78E-71
F7	Best	9.22E-79	8.91E-08	1.54E-06	5.97E-80
	Std	3.08E-66	6.56E-07	7.79E-06	2.63E-69
	Mean	1.23E-01	1.49E+00	1.05E-02	1.09E-01
F8	Best	1.26E-04	1.89E-02	4.09E-03	8.97E-05
	Std	2.42E-03	1.52E-02	4.55E-03	1.46E-03
	Mean	2.03E-03	4.42E-02	1.09E-02	1.50E-03
F12	Best	1.25E-03	4.67E-02	1.00E-02	9.31E-03
	Std	1.12E-02	7.22E-02	2.16E-02	4.44E-02
	Mean	2.11E-01	2.02E+00	1.48E-02	2.09E-01
F15	Best	-1.26E+04	-9.37E+03	-9.91E+03	-1.26E+04
	Std	1.71E+03	9.20E+02	3.89E+02	1.99E+03
	Mean	-1.09E+04	-7.26E+03	-9.04E+03	-1.06E+04
F19	Best	-1.15E+04	-7.34E+03	-9.04E+03	-1.13E+04
	Std	-7.92E+03	-5.18E+03	-8.26E+03	-6.67E+03
	Mean	1.44E-01	1.63E+00	7.78E-03	1.43E-01
F21	Best	6.26E-03	2.13E-01	4.50E-05	5.98E-03
	Std	4.31E-02	4.94E+00	1.91E-02	2.28E-02
	Mean	2.80E-02	6.32E+00	4.06E-03	2.54E-02
F23	Best	1.82E-02	5.29E+00	1.70E-04	1.89E-02
	Std	2.47E-01	2.53E+01	1.05E-01	1.02E-01
	Mean	4.17E-01	2.94E+00	1.44E-02	3.93E-01

To evaluate the convergence performance of the ASWOA algorithm, this section plots the convergence curves for eight algorithms (with parameter settings as above). For the convergence curves of the aforementioned three algorithms, this convergence analysis employs a dimension D=30 and conducts detailed analysis on eight representative test functions (F1, F7, F8, F12, F15, F19, F21, F23) in detail. As shown in Figure 3, each sub-figure corresponds to a test function, with the horizontal axis representing the iteration count and the vertical axis depicting the fitness value of the test function.

The convergence curve comparison illustrates that the introduction of a stagnation counter enables the algorithm to adaptively adjust its global search capability, thereby preventing it from becoming trapped in local optima. Concurrently, the linear adjustment of the dynamic threshold through the decay coefficient further enhances the convergence speed and accuracy of the ASWOA algorithm, significantly improving its overall performance.

Experimental results demonstrate that the ASWOA algorithm exhibits favourable convergence performance across monovalent, polyvalent, hybrid, and composite test functions. Specifically, during testing on F1, F7, F8, F12, F15, F19, F21, and F23, this algorithm not only achieved the highest convergence accuracy but also converged rapidly. It escaped local optima during multiple iterations to attain the optimal value. By contrast, other algorithms demonstrated inferior convergence performance. Furthermore, during the initial iterations, this algorithm rapidly approached or attained the optimal value before gradually converging towards stability. Consequently, in convergence performance comparison tests, ASWOA consistently outperformed other algorithms in overall capability, fully validating the effectiveness of the proposed improvement method for addressing complex optimisation problems.

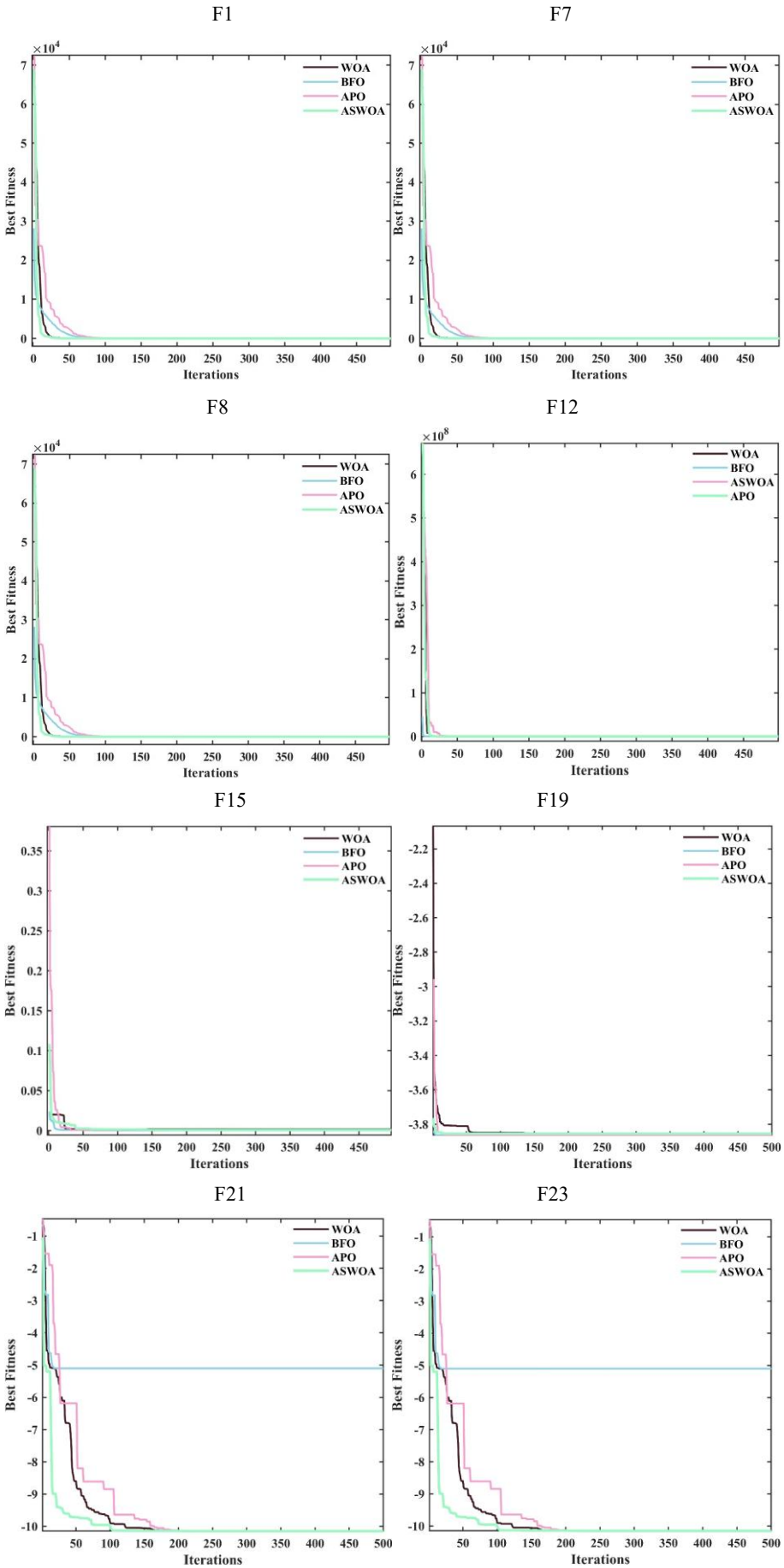

Figure 3. Convergence diagram of benchmark functions.

3. PCA-ASWOA-LSSVM fundamentals

3.1. Principles of Principal Component Analysis (PCA)

Principal Component Analysis (PCA) is a widely adopted technique for dimensionality reduction and for revealing the underlying structure and patterns in high-dimensional datasets. The fundamental principle involves applying a linear transformation to project the original data into a lower-dimensional space where the resulting principal components are uncorrelated with each other and capture most of the variance of the data. The main steps of PCA are summarised as follows:

(1) Normalize the original data.
(2) Calculate the correlation (or covariance) matrix and perform feature decomposition.
(3) Select the first q feature vectors.
(4) The normalised data were projected onto selected eigenvectors to construct principal components.
(5) Calculate the proportion of variance contribution and cumulative variance contribution for each principal component.

Typically, the top q principal components with a cumulative contribution of more than 85% are selected as valid features.

3.2. Principles of Least Squares Support Vector Machine (LSSVM)

LSSVM is an improved variant of the traditional Support Vector Machine (SVM), developed based on the principle of structural risk minimisation. To solve regression problems, LSSVM formulates an optimisation objective by incorporating regularisation theory and the least squares cost function, as defined below:

$$\begin{cases} min\frac{1}{2}\|\omega\|^2 + c\frac{1}{2}\sum_{i=1}^{n}\gamma_i^2 \\ y_i = \omega^T\phi(x_i) + b + \gamma_i \end{cases} \quad (5)$$

Where c denotes the regularisation parameter, which is used to balance the model complexity with the fitting error; γ_i is the ith error term; ω is the vector of weights in the high-dimensional space; φ is a non-linear mapping function from the higher-dimensional space; and b is the bias term.

Based on the construction of the Lagrangian function, the dual regression formulation of the LSSVM can be derived as follows:

$$f(x) = \sum_{i=1}^{n}\eta_j K(x, x_i) + b \quad (6)$$

Where $K(x,x_i)$ needs to satisfy Mercer's theorem. In this study, the radial basis function (RBF) is selected as the kernel function, and its specific formulation is given as follows:

$$K(x, x_i) = exp(-\frac{\|x-x_i\|^2}{2\sigma^2}) \quad (7)$$

where σ is the bandwidth parameter of the RBF kernel, and the final model can be expressed in the following form:

$$f(x) = \sum_{i=1}^{n}\eta_j \times exp(-\frac{\|x-x_i\|^2}{2\sigma^2}) + b \quad (8)$$

Combined with the LSSVM theory, it can be seen that the training effect and generalisation performance of the model are mainly determined by the kernel function parameter σ and the regularisation parameter c together.

3.3. ASWOA optimised LSSVM model

The traditional LSSVM method has obvious defects in parameter optimisation, where the kernel function parameter and regularisation parameters need to be set manually by trial-and-error method or empirical values. This manual adjustment process is not only inefficiency, but also increases the risk that the parameter will be set sub-optimally, leading to overfitting. Moreover, redundant input feature dimensions tend to exacerbate the overfitting, leading to noise in the data fitted to the model, whichreduces the generalisation performance.

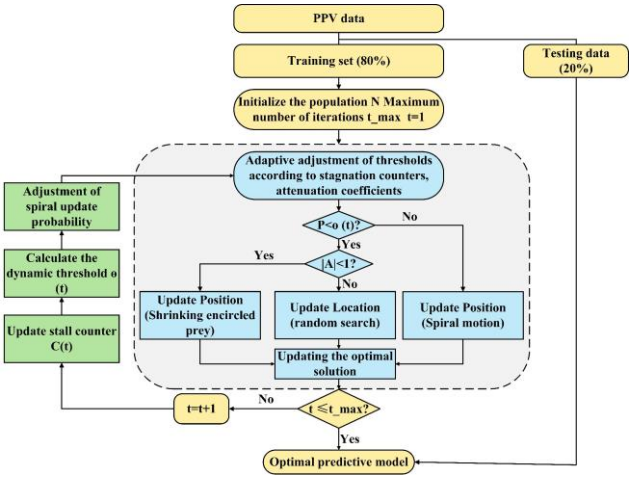

Figure 4. Overall flow chart of the model.

Based on the previously introduced theories of least squares support vector machine (LSSVM), principal component analysis (PCA), and improved adaptive stagnation whale optimisation algorithm (ASWOA), this study proposes a hybrid modelling framework for predicting blasting-induced vibration velocity. PCA is employed to simplify the data structure by eliminating feature redundancy and extracting principal

components that are strongly correlated with the target variables. Subsequently, ASWOA is applied to optimally determine the LSSVM hyperparameters, i.e., the regularisation parameter c and the kernel function parameter σ. Finally, the predicted vibration velocity obtained from the optimised model is compared with the measured data for validation. The detailed implementation process is shown in Fig. 4.

3.4. Model evaluation

Following training and prediction, the performance of the model is evaluateded to verify the accuracy and applicability of the proposed algorithm. In this study, four commonly used performance evaluation metrics are used, namely: the coefficient of determination (R^2), the mean absolute error (MAE), the root mean square error (RMSE), and the mean absolute percentage error (MAPE). The corresponding calculation formulas are presented as follows:

$$R^2 = 1 - \frac{\sum_{i=1}^{N}(y-\hat{y})^2}{\sum_{i=1}^{N}(y-\bar{y})^2} \quad (9)$$

$$MAE = \frac{1}{N}\sum_{i=1}^{N}\left|y-\hat{y}\right| \quad (10)$$

$$RMSE = \sqrt{\frac{1}{N}\sum_{i=1}^{N}(y-\hat{y})^2} \quad (11)$$

$$MAPE = \frac{100\%}{N}\sum_{i=1}^{N}\left|\frac{y-\hat{y}}{y}\right| \quad (12)$$

4. Application of Blasting Vibration Velocity Prediction Model

4.1. Data background

This study collected a total of 78 sets of field-measured blasting vibration data to establish a peak particle velocity (PPV) prediction model. The data were sourced from two tunnel projects with differing geological conditions.

The Guangxi section of the Shennan High-Speed Railway features a tunnel situated within mountainous terrain, with ground elevations ranging from 200 to 430 metres and a maximum burial depth of 275 metres. The tunnel traverses granite formations characterised by hard rock properties yet severely fractured due to tectonic influences, classified as Grade V rock mass. The arch crown and tunnel body exhibit poor stability, presenting challenging engineering geological conditions. The other dataset is taken from the Dianzhong Water Diversion Project (KCT16+910.0 to KCT17+018.5), as documented in reference [17]. This concealed tunnel is driven through amygdaloidal basalt with minor tuff interlayers (Class III rock mass). It intersects two weak fault zones oblique to the tunnel axis, infilled with tuff–mudstone breccia. The presence of buried utilities and building foundations in the shallow overburden further complicates vibration transmission during blasting.

Based on actual field monitoring, five key parameters were selected as the influencing factors of peak particle velocity (PPV): the distance from the blasting centre to the monitoring point (m), the maximum charge single section charge (kg), the total blasting charge (kg), the elevation (m), and the blast hole depth (m). The PPV was taken as the output variable of the prediction model. The data distribution is summarized in Table 4.

Table 4. Blasting vibration data of Kunming section of Dianzhong water diversion project.

Number	Distance from the blast center /m	Elevation /m	Total blasting charge /kg	Maximum single section charge /kg	Hole depth/m	PPV /(cm·s^{-1})
1	14.01	51.03	55	3.4	2.5	0.265
2	24.12	47.89	55	3.4	2.5	0.409
3	19.59	16.57	46	3.4	2	1.261
4	18.22	18.45	62	5	3	1.104
5	19.46	47.07	51	2.4	2	0.402
6	25.22	8.17	46	2.4	2	1.522
7	19.53	46.53	51	4	2	0.387
8	26.06	36.63	51	4	2	0.613
9	9.89	36.17	60	4	3	0.402
10	18.05	35.6	60	4.	3	0.509
…	…	…	…	…	…	…
75	29.7	22.23	90	4.5	3	0.702
76	19.58	31.36	75	3.6	2.5	0.358
77	26.73	19.5	87	5.1	3.5	0.858
78	23.62	21.84	72	3.6	2.5	0.403

4.2. Feature selection

The input data were first randomly shuffled and then divided into training and test sets, with 80% used for training and 20% for testing. The five input variables—distance from the blasting centre to the monitoring point (R), elevation (H), total blasting charge (Q), maximum charge single section charge (C), and blast hole depth (L)—were selected as influencing factors for blasting vibration. These variables were standardised and then subjected to principal component analysis (PCA), where they were transformed into a set of uncorrelated but representative principal components. The correlation matrix of the standardised variables was computed, and the results are presented in Fig. 5.

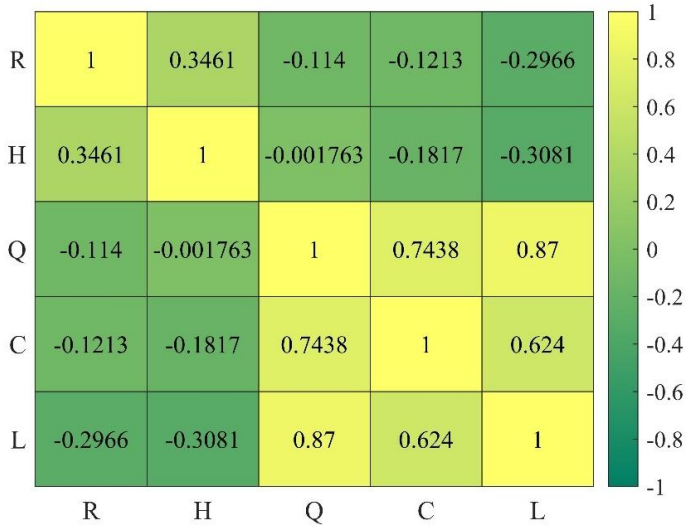

Figure 5. Heat map matrix of correlation of influencing factors.

As shown in Fig. 5, the correlation coefficient between the total blasting charge and the blast hole depth is 0.883, and the correlation coefficient with the maximum charge single section is 0.749, indicating a strong positive correlation between the two. In contrast, its correlation with elevation and the distance from the blasting centre to the monitoring point is relatively weak, at 0.0778 and -0.124, respectively.

The correlation between elevation and the maximum charge single section charge is 0.022, while the correlation with blast hole depth is -0.203, both of which indicate very little linear relationship. Furthermore, the correlation between blast hole depth and distance from the blast centre is -0.275 and the correlation with the maximum charge single section is 0.635. These results indicate that the greater blast hole depth, the greater the single charge usually required, which in turn increases the total blasting charge. This strong interdependence among hole depth, single charge, and total charge highlights their joint contribution to blasting dynamics.

The correlation between blast hole depth and the maximum single blast charge is slightly weaker than that with the total blasting charge, which may be attributed to variations in rock stratification, geological heterogeneity, and other site-specific conditions. Additionally, the correlation coefficient between the distance from the blasting centre to the monitoring point and the elevation is -0.003, indicating virtually no linear relationship between the two variables in this dataset.

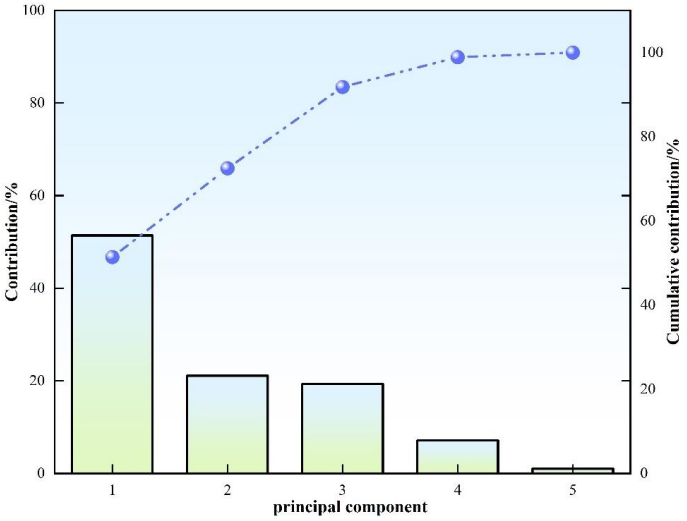

Figure 6. Variance contribution rate and cumulative contribution rate of each principal component.

Based on the matrix of correlation coefficient and an understanding of the blasting mechanism, it can be seen that some input variables show strong interdependence while others show insignificant relationships. Therefore, the application of Principal Component Analysis (PCA) can eliminate weak correlations or redundant features, effectively reducing data complexity, and improve the robustness of the predictive model. PCA was used to reduce the feature dimensionality of the dataset. The explained variance and cumulative contribution of each principal component are illustrated in Fig. 6. The first principal component alone accounts for 51% of the total variance and represents the core of the data structure. By the third principal component, the cumulative explained variance reaches 91.8%, indicating that these three components effectively retain most of the original information. In contrast, each of the remaining component less than 2% of the variance,

indicating that they provide very little additional information. Therefore, we chose the first three principal components to construct the input matrix of the predictive model, thus reducing the dimensionality while retaining the basic data features. Subsequently, based on their respective explained variance and cumulative contributions, the corresponding eigenvectors were derived and the score coefficients for each principal component were computed, as shown in Table 5.

Table 5. Principal component score coefficients.

Characteristic parameter	Principal component 1	Principal component 2	Principal component 3
Distance from the blast centre /m	-0.181	0.209	0.945
Elevation /m	-0.038	0.936	-0.257
Total blasting charge /kg	0.591	0.158	0.114
Maximum single section /kg	0.527	0.155	0.169
Hole depth /m	0.582	-0.175	0.007

Based on the data in Table 5, the principal component expressions can be expressed as follows:

$$\begin{cases} F_1 = -0.181x_1 - 0.0379x_2 + 0.591x_3 + 0.527x_4 + 0.582x_5 \\ F_2 = 0.209x_1 + 0.936x_2 + 0.158x_3 + 0.155x_4 - 0.175x_5 \\ F_3 = 0.945x_1 - 0.257x_2 + 0.114x_3 + 0.169x_4 + 0.007x_5 \end{cases} \quad (13)$$

Where: $x_1 \sim x_5$ are the normalised values of the five input feature variables, respectively.

According to the score coefficients of the first three principal components, F_1 is mainly related to the total blasting charge (Q), the maximum single section charge (C), and the blast hole depth (L). It accounts for 51.4% of the total variance, highlighting the main influence of the blasting design parameters on the generated vibration velocity. Similarly, F_2 is mainly determined by elevation (H), explained 21% of the variance, while F_3 accounts for 19.3% of the variance. This suggests that factors related to topography and the spatial distribution of blasting points have a secondary effect on vibration velocity, compared to the core blasting parameters.

The physical significance of the principal components and their relationship with vibration velocity can be further understood by examining the distribution of the projected data points in the three-dimensional principal component feature space (PC1–PC2–PC3). In Fig. 7, the data points are colour-coded according to their corresponding vibration velocity values, revealing potential patterns and correlations within the reduced feature space.

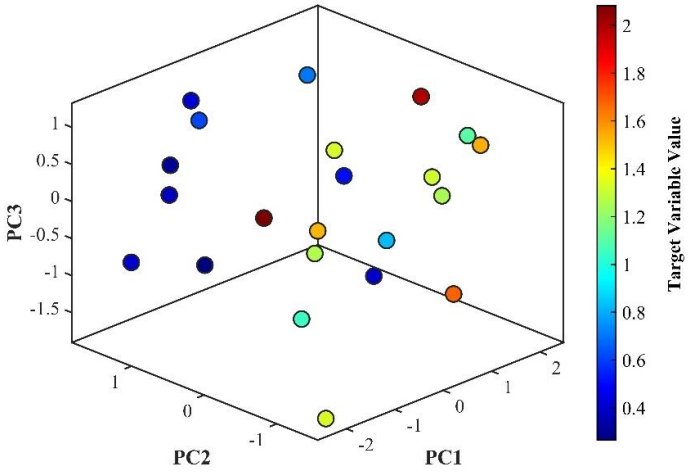

Figure 7. Three-dimensional spatial distribution of principal components.

As can be seen from Fig. 7, along the PC1 axis (total charge, hole depth, maximum single section charge) the value increases, the vibration velocity increases, reflecting the total charge, hole depth and other blasting parameters on the vibration velocity of the significant impact; PC2 (elevation) and PC3 (the distance from blasting centre to monitored point) of the distribution of no significant gradient change, indicating that the two on the blasting vibration velocity of the influence of the weaker or by the influence of other factors lead to.

4.3. PCA-based hyperparameter optimisation of ASWOA-LSSVM

To assess the influence of PCA-based dimensionality reduction on the optimization performance of WOA and ASWOA, LSSVM models were trained using two feature representations: the original input and the first three principal components extracted via PCA.

All optimizations were performed with a population size of 30 and a maximum iteration limit of 400. The ASWOA algorithm adapts its exploration-exploitation balance via the parameter: $\theta(t) = max(0.5 - \delta C(t), 0.1)$

Where θ_{min} =0.1, C_{max}=5 and δ=0.08 (derived from (0.5-θ_{min})/C_{max}). The LSSVM model hyperparameters t = (c, σ) were tuned to minimize the 5-fold cross-validated RMSE (CV-RMSE), computed as:

$$CV - RMSE = \sqrt{\frac{1}{N}\sum_{k=1}^{5}\sum_{i=1}^{n_k}\left(y_i^{(k)} - \hat{y}_i^{(k)}(t)\right)^2} \quad (14)$$

Where $N = \sum_{k=1}^{5} n_k$ is the total number of samples, $y_i^{(k)}$

and $\hat{y}_i^{(k)}(t)$, denote the true and predicted values in the k-th fold, respectively. Results reported are based on the best run (lowest final RMSE) from five independent trials with different random seeds, ensuring robustness against stochastic variation.

For the aforementioned two feature sets, WOA and ASWOA were respectively employed to optimise the hyperparameters c and σ of the LSSVM model, resulting in the construction of four models: WOA-LSSVM and ASWOA-LSSVM based on the original data, alongside PCA-WOA-LSSVM and PCA-ASWOA-LSSVM based on PCA-dimension-reduced data. All experiments were conducted within the MATLAB R2023b environment, with computational platform specifications detailed in Section 2.4. Model performance was primarily evaluated using the 5-fold cross-validation root mean square error (5-fold CV-RMSE) as the primary metric.

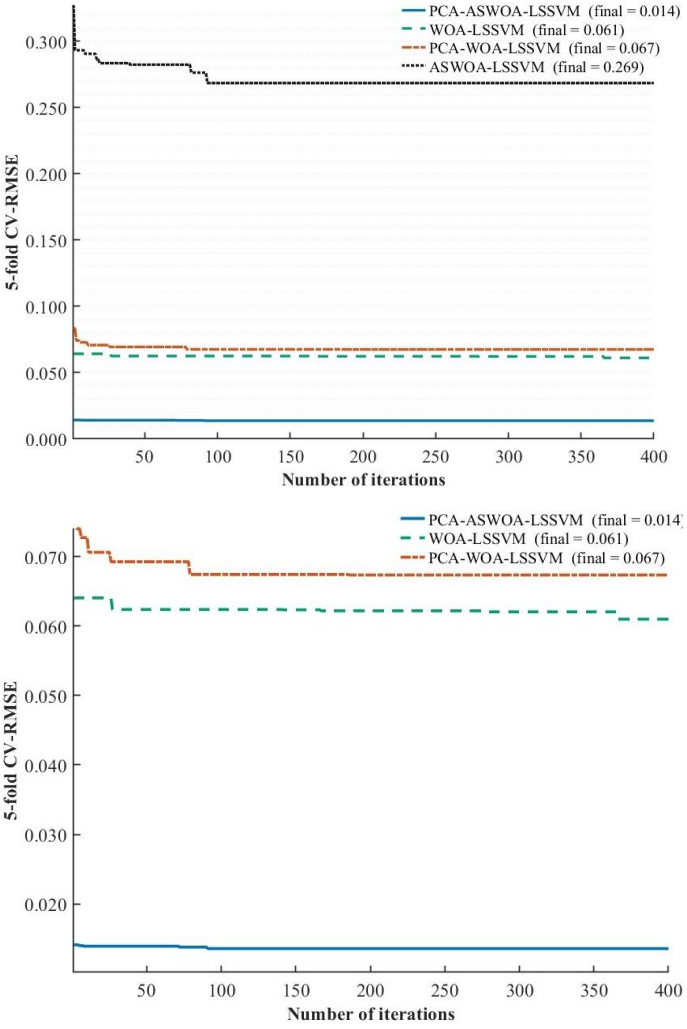

Figure 8. Comparison of the convergence curves of the fitness functions of different optimization models.

In contrast, for the PCA-processed data, the first three principal components were selected as input features. The same optimisation process was applied using WOA and ASWOA, and the resulting optimal parameter sets were used to train the corresponding models. The variation in the values of four fitness evaluation metrics over successive iterations is illustrated in Fig. 8.

The convergence behavior of all four models is illustrated in Fig. 8. During the initial 100 iterations, the CV-RMSE of all models decreased rapidly. The PCA dimensionality reduction model stabilises earlier and achieves lower final errors: PCA-ASWOA-LSSVM converges to 0.014, while PCA-WOA-LSSVM reaches 0.067. In contrast, the original feature models exhibit final RMSEs of 0.269 (ASWOA-LSSVM) and 0.061 (WOA-LSSVM). The RMSE of PCA-ASWOA-LSSVM was reduced by 0.255 compared to the non-PCA version, indicating that combining PCA with ASWOA significantly enhances optimisation performance. Its 0.053 advantage over PCA-WOA-LSSVM also confirms the benefit of ASWOA's adaptive stagnation mechanism in accelerating convergence.

In terms of optimisation efficiency, the PCA-ASWOA-LSSVM model reaches convergence in 91 iterations, compared to PCA-WOA-LSSVM, ASWOA-LSSVM, and WOA-LSSVM which require 186, 93, and 366 iterations respectively. Moreover, WOA-LSSVM reached the next plateau at 366 iterations, and it remains unclear whether convergence is achieved by 400 iterations. This indicates that the PCA-ASWOA-LSSVM model not only improves the prediction accuracy, but also significantly reduces the training and optimisation time.

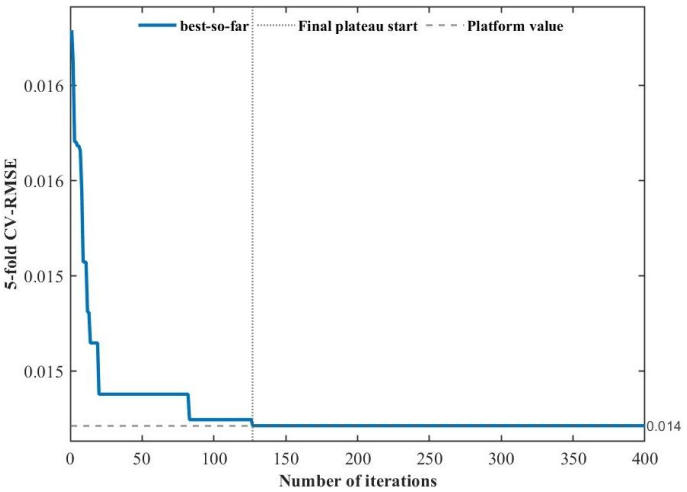

Figure 9. ASWOA Convergence Curve(besr-so-far).

To further analyse the convergence dynamics of the optimal model (PCA-ASWOA-LSSVM), Figure 9 presents its

'historical optimum' 5-fold CV-RMSE curve. Based on the 95% improvement criterion (i.e., achieving 95% of the total improvement relative to the initial solution), the objective function entered a plateau phase at approximately 125 iterations (plateau value: 0.014). Continuing iterations to 400 yields less than 0.1% relative improvement, with no change in external test set performance. Therefore, 400 iterations represent a conservative upper bound; early stopping near the plateau significantly conserves computational resources without compromising accuracy.

Based on the dataset in Table 4, 62 samples were randomly selected for model training and remaining 16 samples were used as an independent test set for evaluating the prediction performance. After 400 iterations, the optimal hyperparameter values were determined to be c=14.97 and σ=2.44. Fig. 10 illustrated the fitted regression curves based on training set. The results show that the PCA-ASWOA-LSSVM model has high predictive accuracy.

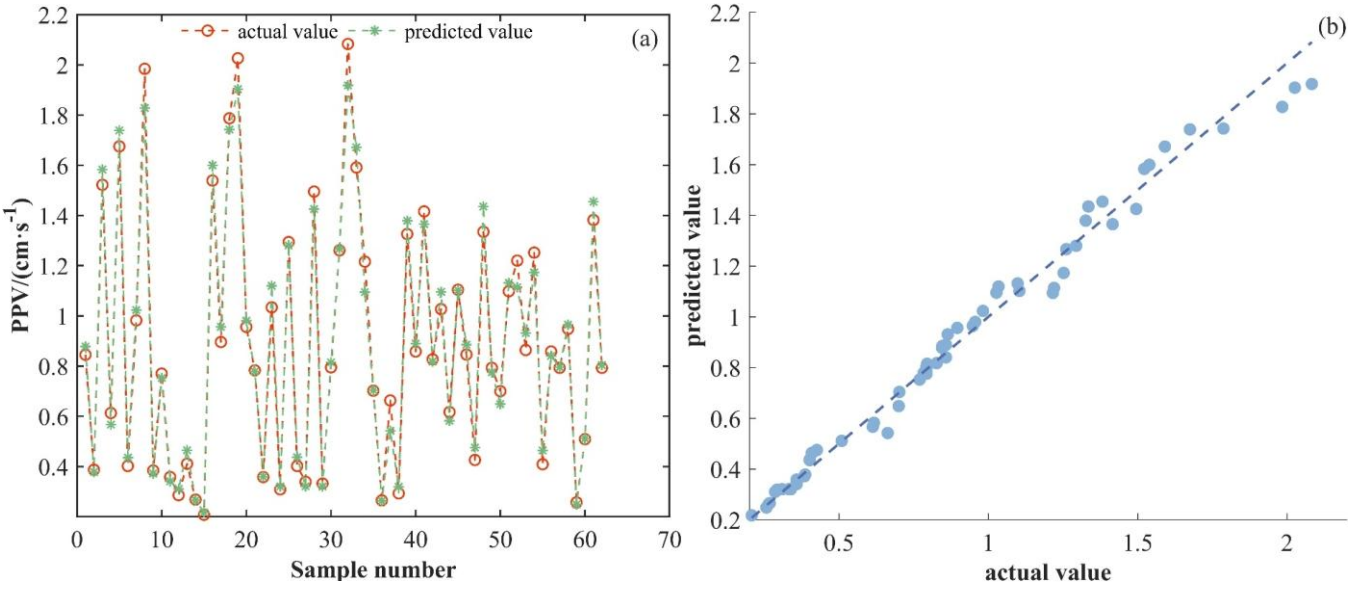

Figure 10. PCA-ASWOA-LSSVM training sample fitted regression curve. (a) Distribution of sample prediction errors; (b) Scatterplot of predicted values fitted to actual values.

4.4. Results of different model training

To evaluate the prediction accuracy of the PCA-ASWOA-LSSVM model, we compared its performance with five benchmark models: the standard Least Squares Support Vector Machine (LSSVM), the Backpropagation (BP) neural network, the WOA-LSSVM model, the ASWOA-LSSVM model, and the PCA-WOA-LSSVM model. Among these, the BP neural network configuration employs a MATLAB newff feedforward network with one hidden layer (64 neurons, selected via 5-fold × 3-fold cross-validation). The hidden layer uses the tansig activation function, while the output layer employs purelin. Training function: `trainbr` (Bayesian regularisation), with a maximum of 400 iterations, target MSE 1×10^{-6}, `min_grad`=1×10^{-6}. Input/output normalisation applied using `mapminmax[0,1]` (only during training set/training fold fitting). Data split 80/20. CV random seed 2025–2027. All models were evaluated under a uniform data partitioning strategy to ensure consistency and fairness in comparison.

The predictive performance of each model was assessed using four standard metrics: coefficient of determination (R^2), mean absolute error (MAE), root mean square error (RMSE), and mean absolute percentage error (MAPE). The results of this comparative analysis are presented in Table 6.

Table 6. Analysis of vibration velocity prediction results of different models.

Training model	Evaluation indicators			
	R^2	MAE	RMSE	MAPE/%
BP	0.529	0.309	0.414	40.8
LSSVM	0.611	0.252	0.321	27.88
WOA-LSSVM	0.637	0.262	0.343	33.78
ASWOA-LSSVM	0.77	0.178	0.218	26.53
PCA-WOA-LSSVM	0.824	0.176	0.207	20.12
PCA-ASWOA-LSSVM	0.966	0.042	0.052	7.02

4.5. Comparison of the prediction effect of different models

Sixteen data sets were randomly selected and trained using six models, namely BP, LSSVM, WOA-LSSVM, ASWOA-LSSVM, PCA-WOA-LSSVM, and PCA-ASWOA-LSSVM. The prediction results are shown in Fig. 11. It is evident from the figure that the PCA-ASWOA-LSSVM model yields predictions that are closest to the measured values, demonstrating the best overall predictive performance.

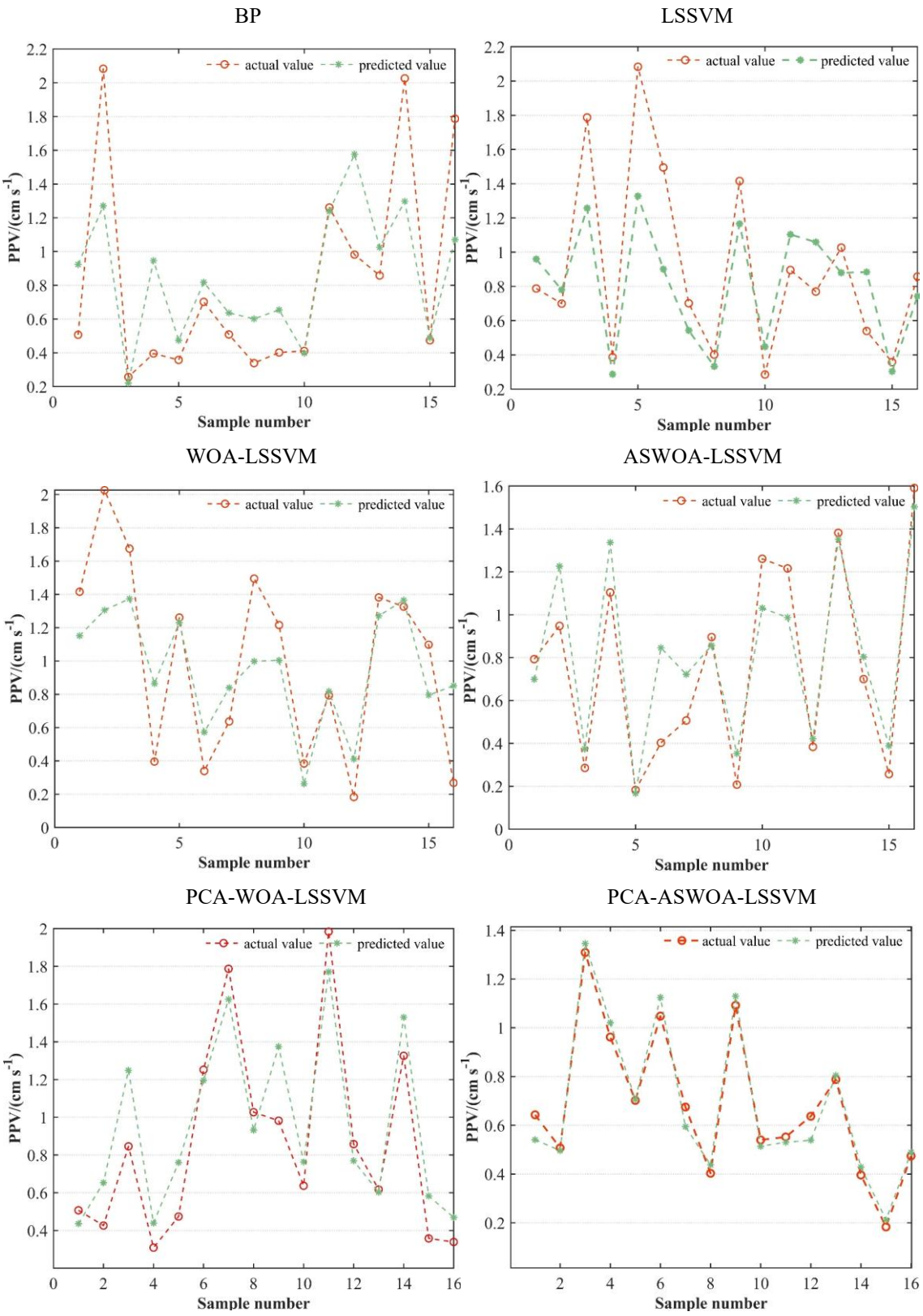

Figure 11. Comparison of predicted and measured values of different models.

The prediction errors of the six models are further analysed and shown in Fig. 12. The maximum error observed for each model is as follows: PCA-ASWOA-LSSVM (15.86%), PCA-WOA-LSSVM (62.85%), ASWOA-LSSVM (109.93%), WOA-LSSVM (217.54%), LSSVM (56.64%), and BP neural network (139.39%). In terms of average error percentage, the PCA-ASWOA-LSSVM model achieved the lowest average error of 7.02%, outperforming the PCA-WOA-LSSVM (20.12%), WOA-LSSVM (33.78%), LSSVM (27.88%), ASWOA-LSSVM (26.53%), and BP (40.8%) models.

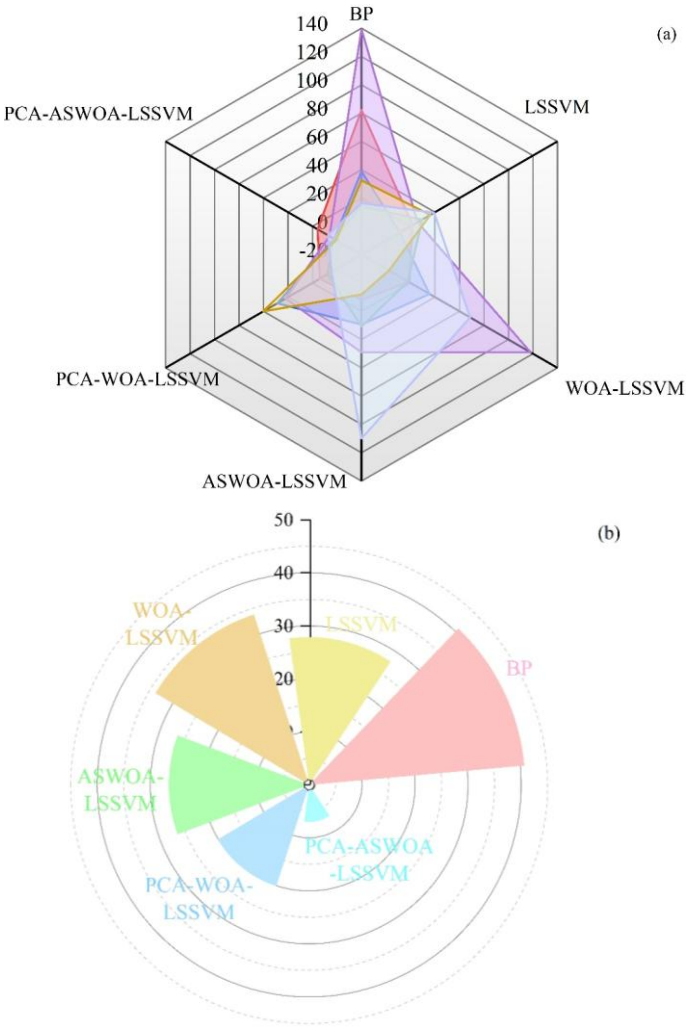

Figure 12. Model error analysis. (a) Percentage of error; (b) Average percentage of error.

These results show that the PCA-ASWOA-LSSVM model not only achieves the highest prediction accuracy, but also demonstrates the best agreement with the measured peak vibration velocity values, thus demonstrating excellent generalisation performance.

5. Conclusions

To improve the prediction of vibration velocity induced by tunnel blasting, this study proposes a novel ensemble prediction model. The model integrates principal component analysis (PCA), an adaptive stagnation whale optimisation algorithm (ASWOA), and least squares support vector machine (LSSVM). In tunnel blasting vibration prediction, the model principal component analysis (PCA) is applied to extract key features that influence vibration velocity. This approach reduces the complexity of input variables. It also simplifies the training process of the LSSVM model. At the same time, most of the essential information from the original data is retained. Consequently, the model's predictive accuracy and generalization are significantly improved.

To overcome the limitations of the traditional whale optimisation algorithm (WOA), namely the limited global exploration capability and a tendency to converge prematurely to local optima, an improved variant, termed the Adaptive Stagnation Whale Optimisation Algorithm (ASWOA), is proposed. The algorithm dynamically adjusts the activation probability of the spiral update mechanism, thereby enhancing exploration and exploitation capabilities. Experimental results show that ASWOA has faster convergence, better global search performance, and better ability to escape from local optima than the standard WOA.

The PCA-ASWOA-LSSVM hybrid model demonstrates superior overall predictive performance compared to other models, including PCA-WOA-LSSVM, ASWOA-LSSVM, BP, WOA-LSSVM, and LSSVM. Specifically, it achieves the highest coefficient of determination (R^2), with an improvement of 0.437. The root mean square error (RMSE) is reduced by 0.362. The mean absolute error (MAE) decreases by 0.267, the mean absolute percentage error (MAPE) drops by 33.78%. The research conclusion shows that the adaptive stagnation model presented in this paper enhances the prediction performance of blasting vibration, while maintaining stability. This contributes to the safety and stable operation of tunnel blasting construction.

Acknowledgment

This work was supported by the National Natural Science Foundation of China (52478525), Key Technologies Research and

Development Program of HuBei Province (2024DJC006), Graduate Scientific Research Foundation of Jianghan University (KYCXJJ202439). The supports are gratefully acknowledged.

Declaration of competing interest

The authors declare that they have no known competing financial interests or personal relationships that could have appeared to influence the work reported in this paper.

References

1. Xie X Q, Huang X W, Yao Y K, Li H, Yue W. Study prospect of precision blasting technology in open-pit deep hole bench. Metal Mine 2022; (7): 7–18. doi:10.19614/j.cnki.jsks.202207002.
2. Kang Y, Yao Y, Dong R, Jia Y, Xie Q, Wang J. Improved complete ensemble empirical mode decomposition with adaptive noise and composite multiscale permutation entropy for denoising blast vibration signal. Heliyon 2024; 10(18): e37339, https://doi.org/10.1016/j.heliyon.2024.e37339.
3. Yao Y K, Zhang C, Nie S L, Wang W. Test and analysis of vibration characteristics induced by blasting demolition of reinforced concrete support beam. Blasting 2023; 40(1): 108-114. doi:10.3963/j.issn.1001-487X.2023.01.015.
4. Xu G, Wang X. Support vector regression optimized by black widow optimization algorithm combining with feature selection by MARS for mining blast vibration prediction. Measurement 2023; 218: 113106, https://doi.org/10.1016/j.measurement.2023.113106.
5. Sun M, Yang J, Yang C, Wang W, Wang X, Li H. Research on prediction of PPV in open-pit mine used RUN-XGBoost model. Heliyon 2024. doi:10.1016/j.heliyon.2024.e28246, https://doi.org/10.1016/j.heliyon.2024.e28246.
6. Duvall WI, Fogelson D E. Review of criteria for estimating damage to residences from blasting vibrations. US Department of the Interior, Bureau of Mines; 1962.
7. Gao Y, Fu H, Rong X, Paneiro G. Ground-borne vibration model in the near field of tunnel blasting. Applied Sciences 2022; 13(1): 87. doi:10.3390/app13010087.
8. Bai R, Zhang P, Zhang Z, Sun X, Fei H, Bao S, Hu G, Li W. Optimization of blasting parameters and prediction of vibration effects in open pit mines based on deep neural networks. Alexandria Engineering Journal 2023; 70: 261–271, https://doi.org/10.1016/j.aej.2023.02.043.
9. Yuan H, Zou Y, Li H, Ji S, Gu Z, He L, Hu R. Assessment of peak particle velocity of blast vibration using hybrid soft computing approaches. Journal of Computational Design and Engineering 2025; 12(2): 154–176, https://doi.org/10.1093/jcde/qwaf007.
10. Zhou X. Construction of environmental vibration prediction model for subway transportation based on machine learning algorithm and database technology. Scientific Reports 2024; 14(1): 6288, https://doi.org/10.1038/s41598-024-56940-3.
11. Hu N, Kong L, Zheng H, Zhou X, Wang J, Tao J, Li W, Lin J. Trend Prediction of Vibration Signals for Pumped-Storage Units Based on BA-VMD and LSTM. Energies 2024; 17(21): 5331, https://doi.org/10.3390/en17215331.
12. Nguyen H, Choi Y, Bui X-N, Nguyen-Thoi T. Predicting Blast-Induced Ground Vibration in Open-Pit Mines Using Vibration Sensors and Support Vector Regression-Based Optimization Algorithms. Sensors 2020; 20(1): 132, https://doi.org/10.3390/s20010132.
13. Chen W, Hasanipanah M, Nikafshan Rad H, Armaghani D J, Tahir M M. A new design of evolutionary hybrid optimization of SVR model in predicting the blast-induced ground vibration. Engineering with Computers 2021; 37(2): 1455–1471, https://doi.org/10.1007/s00366-019-00895-x.
14. Yang H, Nikafshan Rad H, Hasanipanah M, Amnieh H B, Nekouie A. Prediction of Vibration Velocity Generated in Mine Blasting Using Support Vector Regression Improved by Optimization Algorithms. Natural Resources Research 2020; 29(2): 807–830, https://doi.org/10.1007/s11053-019-09597-z.
15. Wang Y, Wang J, Zhou X, Zhao T, Gu J. Prediction of Blasting Vibration Intensity by Improved PSO-SVR on Apache Spark Cluster. In Shi Y, Fu H, Tian Y et al. (eds): Computational Science – ICCS 2018, Cham, Springer International Publishing: 2018: 748–759, https://doi.org/10.1007/978-3-319-93701-4_59.
16. Zhang Y, Wang L. Real-Time Fault Monitoring Method for Logistics Vehicles Based on Chaotic Ant Colony Algorithm. Eksploatacja i Niezawodność – Maintenance and Reliability 2025; 27(4): 7. doi:10.17531/ein/203395.
17. Zhang G P, Zhao G, Hu Y G, Haowen Z, Yu R, Zhaowei Y. Predicting Peak Velocity of Blasting Vibration Using BFO-LSSVM Algorithm.

Technology and Economy of Changjiang 2022; 6(5): 51–56. doi:10.19679/j.cnki.cjjsjj.2022.0509.
18. Weng W, Zhang M, Zhao Y, Wang H. Prediction of blast vibration velocity based on multi-model dynamic weighting ensemble. Mechanics of Advanced Materials and Structures 2025; 1–18, https://doi.org/10.1080/15376494.2025.2496758.
19. Xu S, Li Y, Liu J, Zhang F. Optimization of blasting parameters for an underground mine through prediction of blasting vibration. Journal of Vibration and Control 2019; 25(9): 1585–1595, https://doi.org/10.1177/1077546319829938.
20. Komadja G C, Rana A, Glodji L A, Anye V, Jadaun G, Onwualu P A, Sawmliana C. Assessing Ground Vibration Caused by Rock Blasting in Surface Mines Using Machine-Learning Approaches: A Comparison of CART, SVR and MARS. Sustainability 2022; 14(17): 11060, https://doi.org/10.3390/su141711060.
21. Faradonbeh R S, Monjezi M. Prediction and minimization of blast-induced ground vibration using two robust meta-heuristic algorithms. Engineering with Computers 2017; 33(4): 835–851, https://doi.org/10.1007/s00366-017-0501-6.
22. Zhou S, Zhang Z-X, Luo X, Niu S, Jiang N, Yao Y. Developing a hybrid CEEMDAN-PE-HE-SWT method to remove the noise of measured carbon dioxide blast wave. Measurement 2023; 223: 113797, https://doi.org/10.1016/j.measurement.2023.113797.
23. Zhang X, Zhu C, He M, Dong M, Zhang G, Zhang F. Failure Mechanism and Long Short-Term Memory Neural Network Model for Landslide Risk Prediction. Remote Sensing 2022; 14(1): 166, https://doi.org/10.3390/rs14010166.
24. Hasanipanah M, Monjezi M, Shahnazar A, Armaghani D J, Farazmand A. Feasibility of indirect determination of blast induced ground vibration based on support vector machine. Measurement 2015; 75: 289–297, https://doi.org/10.1016/j.measurement.2015.07.019.
25. Liu Q, Sun R, Bu X, Hanajima N, Ding W. Optimal Trajectory Planning Method for Handling Robots Based on Multi-objective Particle Swarm Optimization Guided by Evolutionary Information. Eksploatacja i Niezawodność – Maintenance and Reliability. 2025; 27(4): 4. doi:10.17531/ein/202990.
26. Bui X-N, Nguyen H, Tran Q-H, Nguyen D-A, Bui H-B. Predicting Blast-induced Ground Vibration in Quarries Using Adaptive Fuzzy Inference Neural Network and Moth–Flame Optimization. Natural Resources Research 2021; 30(6): 4719–4734, https://doi.org/10.1007/s11053-021-09968-5.
27. Hosseini S, Khatti J, Taiwo B O, Fissha Y, Grover K S, Pushkarna M, Berhanu M, Ali M. Assessment of the ground vibration during blasting in mining projects using different computational approaches. Scientific Reports 2023; 13(1): 18582, https://doi.org/10.1038/s41598-023-46064-5.
28. Zhou J, Asteris P G, Armaghani D J, Pham B T. Prediction of ground vibration induced by blasting operations through the use of the Bayesian Network and random forest models. Soil Dynamics and Earthquake Engineering 2020; 139: 106390, https://doi.org/10.1016/j.soildyn.2020.106390.
29. Huang Y, Zhou Z, Li M, Luo X. Prediction of Ground Vibration Induced by Rock Blasting Based on Optimized Support Vector Regression Models. Computer Modeling in Engineering & Sciences 2024; 139(3): 3147–3165, https://doi.org/10.32604/cmes.2024.045947.